

Health monitoring of reinforced concrete slabs subjected to earthquake-type dynamic loading via measurement and analysis of acoustic emission signals

Antolino Gallego*¹, Amadeo Benavent-Climent² and Cristóbal Infantes¹

¹*Department of Applied Physics, University of Granada, 18071 Granada, Spain*

²*Department of Mechanics of Structures, University of Granada, 18071 Granada, Spain*

(Received June 21, 2010, Revised November 22, 2010, Accepted July 31, 2011)

Abstract. This paper discusses the applicability of Acoustic Emission (AE) to assess the damage in reinforced concrete (RC) structures subjected to complex dynamic loadings such as those induced by earthquakes. The AE signals recorded during this type of event can be complicated due to the arbitrary and random nature of seismicity and the fact that the signals are highly contaminated by many spurious sources of noise. This paper demonstrates that by properly filtering the AE signals, a very good correlation can be found between AE and damage on the RC structure. The basic experimental data used for this research are the results of fourteen seismic simulations conducted with a shake table on an RC slab supported on four steel columns. The AE signals were recorded by several low-frequency piezoelectric sensors located on the bottom surface of the slab. The evolution of damage under increasing values of peak acceleration applied to the shake table was monitored in terms of AE and dissipated plastic strain energy. A strong correlation was found between the energy dissipated by the concrete through plastic deformations and the AE energy calculated after properly filtering the signals. For this reason, a procedure is proposed to analyze the AE measured in a RC structure during a seismic event so that it can be used for damage assessment.

Keywords: acoustic emission; damage evaluation; reinforced concrete; slab; seismic loads.

1. Introduction

Reinforced concrete (RC) structures located in earthquake-prone areas are susceptible to suffering damage caused by the cyclic loading induced by ground acceleration during seismic events. In an RC structure, damage is not generated only during severe earthquakes that stress the reinforcing steel beyond its elastic limit; moderate tremors that may occur several times during the lifetime of a structure also produce damage of the concrete due to cracking. There are several relevant damage mechanisms in concrete. One is the opening of new cracks or the extension of existing cracks that occurs when the tensile stress exceeds the tensile strength of the concrete. Another is the friction between the planes of fracture after cracking. A third mechanism (not found during the tests conducted for this study) is the concrete cracking under compressive stress. Concrete degradation associated with cracking caused by hundreds of cycles of deformation eventually results in cumulative damage (low-cycle fatigue damage) to the structural RC components, in turn leading to

*Corresponding Author, Dr., E-mail: antolino@ugr.es

a state in which repair becomes necessary. One important consequence of concrete degradation under cyclic loading is the slip between the reinforcing steel bars and the surrounding concrete, which is considered serious damage in RC elements (Yuyama *et al.* 2001).

The RC structure is commonly covered up by non-structural elements such as brick veneers, casings, cement plasters, stuccos, etc., making simple visual inspection very complicated. Even so, visual inspection provides only qualitative information regarding the “apparent” damage suffered by the concrete as expressed by cracks, while structural damage such as that associated with the slip between concrete and reinforcing bars is related to cumulative damage resulting from numerous cycles (Yuyama *et al.* 1999). It is here where non-destructive techniques can play an important role. Among them, the measurement, recording and analysis of Acoustic Emission (AE) signals generated during a test or operation proves very effective as a non-destructive technique to deal with remote or inaccessible parts of a structure. Signal processing and pattern recognition have been extensively used in order to discriminate relevant from non-relevant AE records and correlate emission with the associated failure mechanism (Miller and Hill Eric 2005). The AE technique has been applied to RC elements mostly at the material (concrete) or individual element level (beams, columns) (Yuyama *et al.* 1999, 2001, Miller and Hill Eric 2005, Carpinteri *et al.* 2007, Benavent-Climent 2009, Ohtsu and Watanabe 2001, Zhiwei and Paul 2009, McLaskey 2010, Ohtsu 1991, 1998, Grosse and Ohtsu 2008). Little research has been carried out on assemblages of several structural elements (Carpinteri *et al.* 2007). In the latter case, studies have focused on the AE generated by relatively simple loadings such as the vibrations induced by traffic. One example is the research conducted by Yuyama *et al.* (2001) on the fatigue damage of RC slabs supported along their edges and subjected to cyclic loading (sine-waves and actual live loads in slabs in service). Studies on the application of AE to monitor damage on RC structures subjected to the very complex transient loading induced by earthquakes are very rare. Noteworthy among them is the study conducted recently by Carpinteri *et al.* (2007) on masonry towers affected by regional seismicity.

This paper investigates the applicability of the AE technique to assess the damage of RC slabs supported on columns and subjected to seismic-type cyclic loading. In comparison to the AE measured on an RC structure under static loads or steady-state dynamic loading, in the case of earthquake-type dynamic loads the AE signal is more cumbersome and includes a lot of spurious sources of noise. Thus, the AE signals recorded during a seismic event are extraordinarily complex; and unveiling their relation with the damage accumulated on the structure requires considerable post processing work. This study is focused on developing a criterion for filtering the AE data obtained from the measurement of the AE generated on RC slabs under dynamic seismic-type loading. The proposed criterion allows to distinguish the spurious signals not related to concrete damage from the AE related to concrete cracking. On the basis of the latter, the damage quantified in terms of AE energy and the damage characterized in terms of plastic strain energy dissipated by the concrete are seen to be strongly correlated.

2. Dynamic tests

2.1 Description of the test model

A one-storey (2.8 m height) and one-bay (4.8 m length) prototype structure consisting of an RC slab supported on four box-type steel columns was designed following current Spanish codes

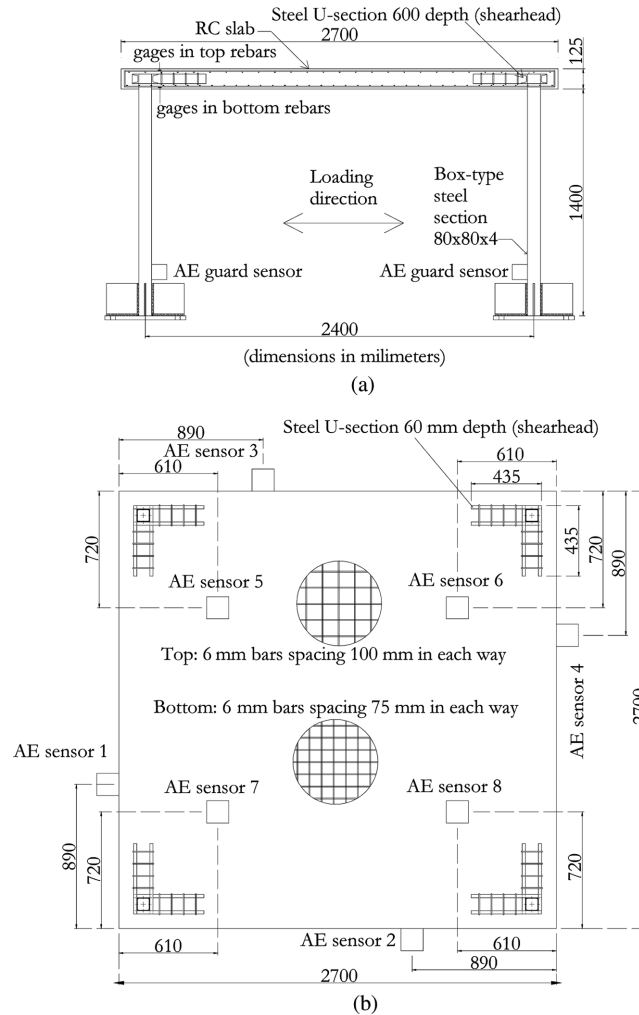


Fig. 1 Test model: (a) elevation and (b) plan

NCSE-02 (2002) and EHE-08 (2008). From the prototype structure, the corresponding test model was derived by applying the following similarity laws: $\lambda_r=1/2$, $\lambda_a=1$ and $\lambda_\sigma=1$, where λ_b , λ_a and λ_σ are the scaling factors by which the geometry, the acceleration and the stress in the prototype must be multiplied to obtain the corresponding dimensions in the test model. Fig. 1 shows the geometry and reinforcing details. The depth of the slab is 125 mm and it is reinforced with steel meshes, one on the top made with 6 mm diameter bars spaced 100 mm, and another on the bottom consisting of 6 mm diameter bars spaced 75 mm. The test model was prepared in the laboratory. The average yield stress f_s of the reinforcing steel was 467 MPa, and the average concrete strength f_c was 23.5 MPa.

2.2 Loading set-up and seismic simulation

The test model was tested with the uniaxial MTS 3x3 m² shaking table of the University of

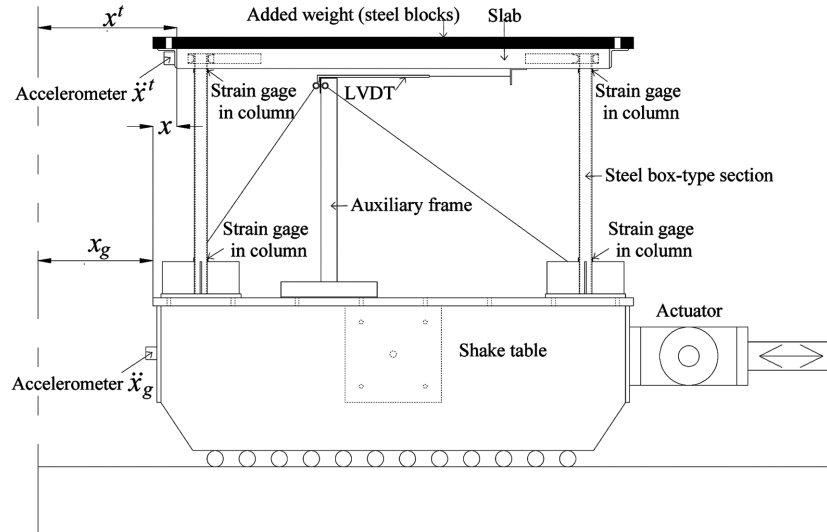


Fig. 2 Experimental set-up

Granada (Spain) shown in Fig. 2. The bottom ends of the columns were fixed to the table by bolts. Similitude requirements between prototype and test model and the dead and live gravity load were satisfied by attaching additional steel blocks on the top of the RC slab. The total mass of the slab including the added steel blocks was $m = 7390$ kg. The inertial force generated in the RC slab and the additional steel blocks when the shake table was accelerated dynamically loaded the test model. The acceleration record used for the shake table tests reproduced the NS component of the 1980 Campano-Lucano earthquake recorded at Calitri (Italy).

Two series of seismic simulations were applied to the test model. The same accelerogram was used in all simulations, the scaling factor of the peak accelerations (PA) being the only difference. The first column of Table 1 shows the PA applied in each simulation. The first series consisted of eight simulations with PA increasing progressively from $0.08 g$ to $0.58 g$ (here g is the acceleration of gravity). The second series consisted of six simulations with PA increasing from $0.19 g$ to $0.95 g$. The second series started with values of PA smaller than the maximum obtained in the first series, that is, in several simulations of the second series the test model was subjected to load levels smaller than those it had been previously exposed to. This was intentionally done so that the simulations reproduced two types of situations on the structure: (i) that in which the AE energy and plastic strain energy are dominated by the new damage associated with the opening and extension of cracks; and (ii) the situation in which AE energy and hysteretic energy are dominated by friction generated from existing damage. Both situations are realistic scenarios that the structure may experience over its lifetime. During the seismic simulations the test model was driven very close to the limit commonly acceptable on an RC structure subjected to moderate earthquakes. The measurements of the strain gages attached to the reinforcing bars (described later in the subsection 2.3) indicated that: (i) the maximum strain in the reinforcing bars $\varepsilon_{max, reinf}$ (see Table 1) closely approached the yield strain ($2200 \mu\varepsilon$); and (ii) slip occurred between the longitudinal reinforcing bars and the surrounding concrete.

Table 1 Seismic simulations

Test series		PA(g)	T (s)	ξ (%)	$\epsilon_{max, reinf}$ ($\mu\epsilon$)
1	2				
Simulation (in order of application)					
A1		0.08	0.26	1.10	497
B1		0.10	0.29	1.14	568
C1		0.12	0.30	1.20	638
D1		0.19	0.31	1.26	909
E1		0.29	0.31	1.30	1150
F1		0.38	0.31	1.42	1361
G1		0.44	0.31	1.48	1537
H1		0.58	0.31	1.60	1670
	A2	0.19	0.32	1.66	836
	B2	0.38	0.32	2.11	1295
	C2	0.58	0.32	2.55	1350
	D2	0.66	0.32	3.16	1460
	E2	0.74	0.32	3.24	1540
	F2	0.95	0.32	3.50	1800

2.3 Displacement, strains and acceleration monitoring

Displacements, strains and accelerations were acquired simultaneously during each seismic simulation. The relative horizontal displacement x between the shake table and the slab was measured by displacement transducers indicated by LVDT in Fig. 2. Electrical resistance strain gages were attached to nineteen - top and bottom - longitudinal reinforcing bars near the corner of the slab prior to casting the concrete as indicated in Fig. 1. Strain gages were also attached at the upper and lower ends of the columns, as shown in Fig. 2. Accelerometers were fixed to the shake table and to the slab as indicated in Fig. 2, which measured the absolute acceleration of the table, \ddot{x}_g , and the absolute response acceleration of the slab, \ddot{x}^f , in the direction of shaking, respectively. All data were collected continuously with a sampling rate of 200 Hz by a data acquisition system. In addition to the electronic data, detailed visual inspections of the slab were made after each seismic simulation to identify the propagation of the cracks.

2.4 Acoustic emission monitoring

A Vallen System ASMY-5 was used to measure the AE signals during the tests. Sixteen AE flat low-frequency sensors were placed on the specimen at the eight positions indicated in Fig. 1 (note that four positions were chosen along the four lateral sides of the specimen, while the other four positions were on the bottom of the specimen). To allow comparison, two sensors were placed at each position, one being type VS30 set in the range 20-100 kHz, and the other type VS75 set in the range 50-140 kHz. In all sixteen channels, the 25-180 kHz frequency band was used during signal acquisition. During acquisition, a sample period of 1.6 μs and 1024 data were used for signal recording (200 of them, before the arrival time). Thus, the entire duration of the record window was

$t_{max} = 1318 \mu s$. Adhesive silicone was used for the coupled fixing of sensors on concrete. Before testing, the electric noise in the laboratory was measured and a calibration test by breaking pencil leads (AE Hsu-Nielsen source) along the specimen was carried out. Thus, it was established that using 45 dB as the threshold of detection, pencil leads broken at any place of the specimen could be recorded by all the sensors.

Attenuation tests were carried out by breaking pencil leads along the specimen, and measuring the signals in all the 16 sensors. Five leads were broken in each position, and the mean level was calculated. Thus it was established that 0.11 dB/m was the mean attenuation. Then, keeping in mind that the point farthest from an AE sensor (the centre of slab) is 94 cm away (distance from the centre to sensors 5, 6, 7 or 8), the maximum attenuation of a source located at that point would be 10.3 dB. Since a threshold of 45 dB was used, it can be stated that all the sources producing AE signals with amplitude higher than 55.3 dB can be recorded by at least one sensor. Note, however, that the centre of the slab is the place where less cracking is expected, since the bending moment under lateral loads is approximately zero.

In general, different modes of propagation can be expected in the acoustic emission waves generated by the cracking of a concrete slab (i.e., longitudinal waves, transversal waves, Rayleigh waves, Lamb waves). These modes of propagation superpose each other and are influenced by many factors such as the mechanics of the damaging process on the concrete. Under earthquake-type cyclic loadings, the concrete experiences both damage associated with the opening (new cracks) and extension of cracks, and damage due to friction between the planes of fracture of previous cracks. Other factors such as the orientation of the cracks, the geometry of the specimen, the type of sensor, the multiple reflexions arising along the wave travel between the source and the sensor etc., play an important role. Most of these factors are random and they can hardly be controlled. All these factors make the signal very cumbersome and modify the vibration modes. The analysis of a complex material such as concrete or of a reinforced concrete structure based on the study of the vibration modes is meaningless, since it is very difficult to identify the different vibration modes.

For the depth of the slab tested in this study (125 mm), the frequency of the propagation modes corresponding to the Lamb waves is below 20 kHz, that is, outside the frequency range of sensitivity of the two types of sensors used. Therefore, it can be concluded that the recorded waves are a mixture of longitudinal and transverse waves. Further, the velocity of propagation of the longitudinal waves was measured by breaking pencil leads, giving an average value (obtained with six measurements) of 3200 m/s.

Due to the complexity of the test and of this type of dynamic loading, a great quantity of undesired friction noise and mechanical noise was expected. For this reason, different precautions were taken to deal with such spurious signals before and after the test. Considerable mechanical noise coming from the oil flow in the actuator that moved the shaking table was detected. The level of this noise was above 100 dB in the actuator, and about 70 dB at the base of the four steel columns that formed the specimen. For this reason, one guard sensor was placed at the bottom of each column, as indicated in Fig. 1, in order to filter this noise and the friction noise generated in the connection between the base plate of the columns and the surface of the shaking table.

Moreover, in an attempt to prevent friction noise generated between the different metallic elements located in the specimen (added steel blocks, screws, fixing systems of sensors, accelerometers, LVDT's, etc.), rubbers and teflon films were inserted between any two contacting surfaces susceptible of generating noise. However, despite these precautions, it was observed that a number of spurious signals, most likely attributable to the oil flow in the actuator that moved the shaking table, were

registered by the sixteen AE sensors. For this reason, it was mandatory to carry out AE data off-line filtering, after the test, as explained in Section 3. Basically, the signals coming from concrete fracture and the signals coming from other sources were discriminated.

3. Proposed procedure for filtering the AE signals

First, a detailed observation of the AE waveforms recorded in all sensors and for all seismic simulations was carried out. Two types of signals were found to be qualitatively different: i) short-duration signals, whose energy was concentrated mainly at the beginning of the signal, and whose duration (D) was not excessively high; and ii) long-duration signals, whose energy was not concentrated at the beginning of the signal, but distributed along the whole signal. It was observed that both types of signals had largely varying durations and amplitudes in dB, a feature complicating their separation by traditional filters based only on the classic parameters of AE signals. Therefore, it was decided to develop a procedure for filtering the signals.

The filtering procedure departs from the premise - based on bibliographical documentation and our own experience with this type of material - that the short-duration signals referred to above as type i correspond to concrete cracking, while the long-duration signals designated as type ii are associated with various spurious sources other than concrete cracking.

The first step of the procedure entailed plotting the amplitude A of the signals versus their duration D as shown in Fig. 3. Each dot in Fig. 3 represents a particular AE signal in the D versus A plane. In general, as expected, D increases with A . By observing the AE waveforms corresponding to each dot of Fig. 3, it was found that the following two regions can be distinguished

$$\text{Region A: AE signals with and } D > [3000 + 80(A - 45)]\mu\text{s and } A < 60 \text{ dB} \quad (1)$$

$$\text{Region B: AE signals with } D \leq [3000 + 80(A - 45)]\mu\text{s or } A \geq 60 \text{ dB} \quad (2)$$

Altogether, 99% of the AE signals located in region A (shaded region in Fig. 3) were characterized by exhibiting a clearly long-duration behaviour, and it was decided to consider these signals as type ii. Fig. 4 illustrates two typical signals of this type (signals 1 and 2). The Eq (1) that defines the region A will be called “**Filter 1**” hereafter. The first inequation of the Eqs. (1) and (2) above are obtained by solving D in the equation of the sloping straight line that passes through the point ($D = 3000 \mu\text{s}$, $A = 45 \text{ dB}$) sloped $0.0125 \text{ dB}/\mu\text{s}$ in the D versus A plane shown in Fig. 3, i.e., $A - 45 = 0.0125 (D - 3000)$.

It is worth noting, however, that very impulsive phenomena might also lead to high amplitude signals with low duration, which may cause significant damage to the structure. In Fig. 3 it is seen that for $D > 3000$, the amplitude A of the signals tends to be linearly linked to the burst duration D . This fact indicates these long-duration signals could be attributed to a common mechanism. As already pointed out, the movement of the piston of the actuator was found to be a source of long-duration noise at the base of the shaking table (where the steel columns of the specimen are fixed), the amplitude of this noise being about 70 dB. Most of this spurious noise was filtered by the four guard sensors installed at the lower end of the columns, but this filtering was not 100% effective. Several of these signals probably reached the 16 sensors located on the concrete slab with much lower amplitude, of 60 dB at most. To this respect, it is worth noting that hits with burst duration $D > 3000$ have amplitudes lower than 60 dB. Therefore, these hits are most likely due to the noise

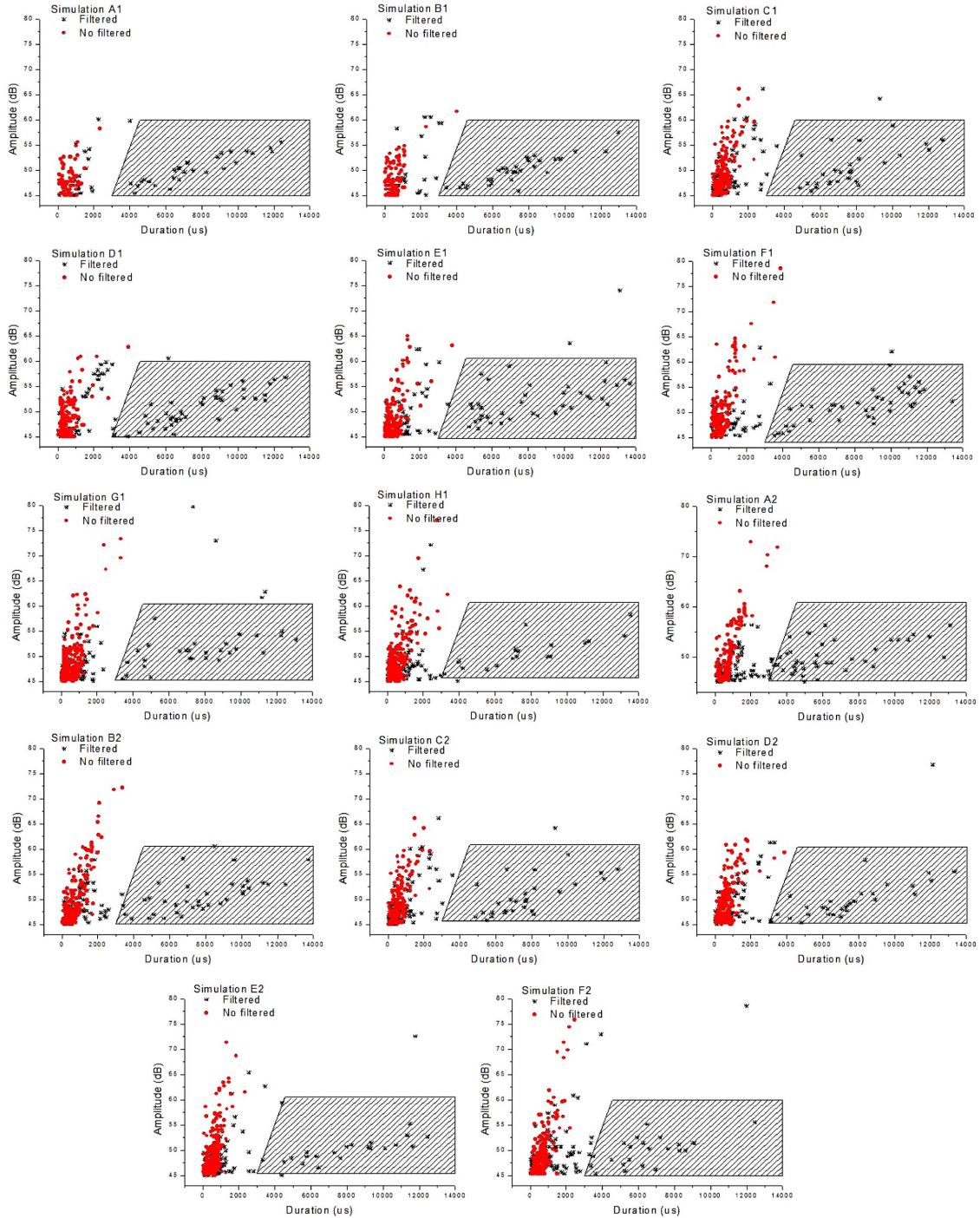


Fig. 3 Amplitude A versus duration D of the AE events recorded during each seismic simulation with VS30 sensors. The black asterisks indicate the events that did not pass the acceptance criteria and were filtered by **Filters 1 and 2**. The red dots indicate the events that did pass the acceptance criteria and were not filtered by **Filters 1 and 2**

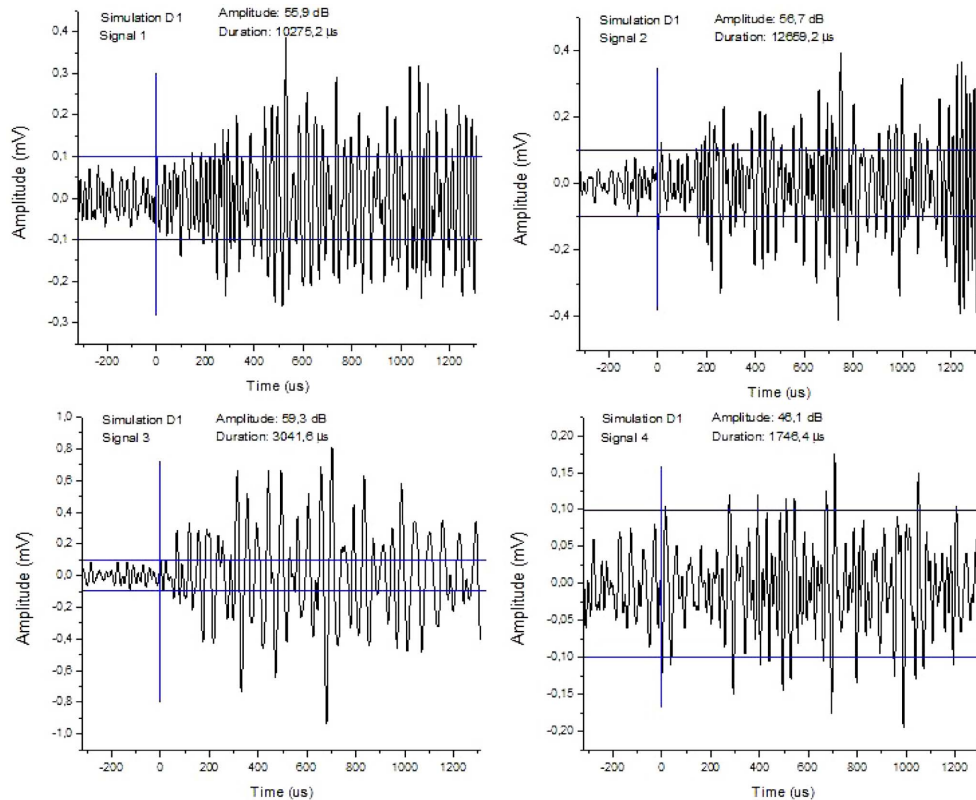


Fig. 4 Signals marked on Fig. 5. Simulation D1. VS30 Sensors. Signals 1 and 2: Type ii signals inside the polygon. Signals 3 and 4: Type ii signals outside the polygon

of the piston of the actuator and not to concrete cracking. These hits were filtered by Filter 1.

However, it was observed that a lot of signals located outside the shaded region delimited by the polygon (Filter 1) also had a clearly long-duration nature (i.e., they were of type ii). As an example, Fig. 4 shows two signals of this type (signals 3 and 4). This means that Filter 1 alone is insufficient. An additional and more sophisticated filter was therefore developed.

As the second step of the procedure, the root mean square (RMS) of all the signals in the following three temporal windows was calculated: $W1$: 0–450 μs , $W2$: 450–1300 μs , and $W3$: 1100–1300 μs . The arrivals of the reflections or other modes depend (with great dispersion) on the distance between the source and sensor and the location of the source in the specimen. For this reason, it was opted to choose a mean value evaluated as the maximum flight time of the fastest propagation mode, i.e., from the centre of the structure (which is equidistant from all the sensors) to the more distant sensor. As the velocity of the fastest mode was 3200 m/s (the longitudinal mode), and the maximum distance between centre of the structure and the sensors was 1.44 m, the maximum flight time is 450 μs . This was the physical criterion used for choosing the duration of window $W1$. This time satisfied the visual checking of the signals.

By denoting as R_1 , R_2 and R_3 the RMS of the signal in each of these three windows, the following filtering criteria were then established: a signal was considered of type i, if $R_1/R_2 \geq 1.0$ and $R_1/R_3 \geq 1.2$; otherwise, the signal was considered as type ii. The first condition acknowledges the fact that if

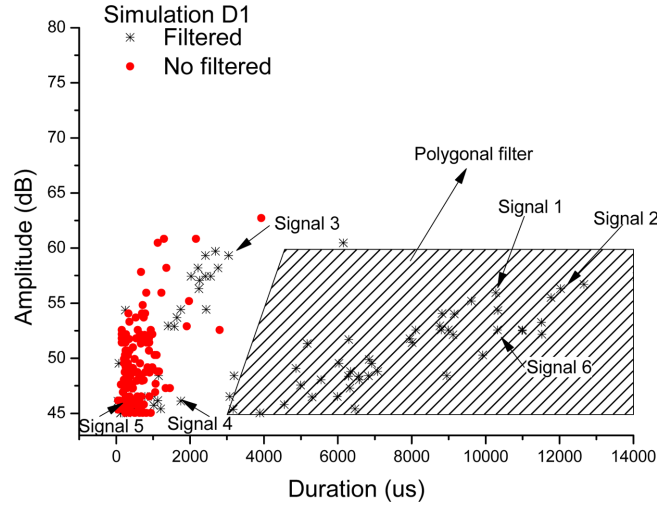


Fig. 5 Signals obtained during simulation *D1* with VS30 sensors. The signals indicated in Figs. 4 and 6 are indicated as “signal 1” through “signal 6”. The black asterisks indicate the events that did not pass the acceptance criteria and were filtered by **Filters 1 and 2**. The red dots indicate the events that did pass the acceptance criteria and were not filtered by **Filters 1 and 2**

a signal is short-duration (i.e., of type i) its RMS should be higher at the beginning of the signal than at the end (i.e., $R_1 > R_2$). The second condition ($R_1/R_3 \geq 1.2$) was introduced in order to filter some long-duration signals with a lot of energy at the end of the waveform. The values 1.0 and 1.2 used in conditions $R_1/R_2 \geq 1.0$ and $R_1/R_3 \geq 1.2$, respectively, were selected so that the difference between the plastic strain energy W_p and the acoustic energy E^{AE} would attain a minimum for the first seismic simulation A1. The filter based on the RMS will be referred to as Filter 2 hereafter.

Fig. 3 shows, in red dots, the signals that did pass the acceptance criteria and not were filtered by Filters 1 and 2, and in black asterisks, the signals that did not pass the acceptance criteria and were filtered by Filters 1 and 2. As an example, Fig. 6 (left) shows a signal that passed both conditions

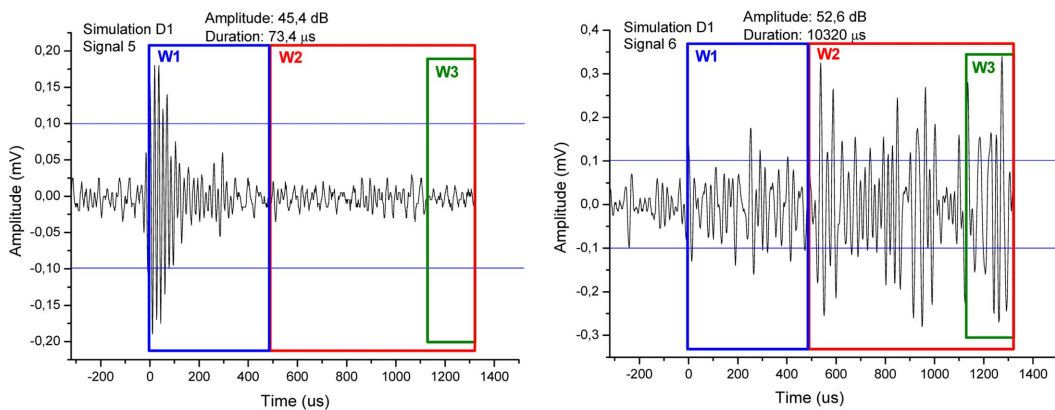


Fig. 6 Signals 5 and 6 marked in Fig. 5, corresponding to simulation *D1*, were recorded with VS30 sensors. Signal 5 was type i while signal 6 was type ii. W_1 , W_2 and W_3 are the temporal windows used to define **Filter 2**

(signal 5). Note that this signal is clearly short-duration. Moreover, Fig. 6 (right) shows a signal that did not pass both conditions (signal 6), which has a clearly long-duration nature.

4. Correlation between the AE energy obtained from the filtered signals and plastic strain energy

The signals passing both conditions were grouped in AE events using the event builder of VisualAE™ software. An event consists of the first and subsequent hits. Over these events, the MARSE energy (energy units; 1ue=1nV·s) of the first hit of the event only, and the accumulated AE energy during each seismic simulation, $(E^{AE})_i$ where i denotes the seismic simulation, were calculated. For each seismic simulation, Fig. 7 shows with dotted lines the history of $(E^{AE})_i$ normalized by the corresponding value at the end of each simulation denoted by $(E^{AE})_{i,end}$.

Meanwhile, by modelling the structure as a single degree of freedom system of mass m and assuming that the inherent damping of the structure is of the viscous type, the equilibrium equation of the system shown in Fig. 2 gives

$$m\ddot{x} + c\dot{x} + F_{spr} = 0 \tag{3}$$

where c defined as

$$c = 4\pi\xi m/T \tag{4}$$

is the viscous damping coefficient and F_{spr} is the restoring force opposed by the structure against the relative displacement x . Here ξ is the damping fraction and T the vibration period, which were estimated experimentally by performing free vibration tests after each simulation. The resulting values of ξ and T are shown in Table 1. Solving for F_{spr} in Eq. (3) gives F_{spr} .

The absolute acceleration \ddot{x} was recorded directly by the accelerometer attached to the slab and the relative velocity \dot{x} was calculated by deriving the relative displacement measured by the LVDT with respect to time. Proceeding in this way, the restoring force F_{spr} was obtained for each seismic simulation and the corresponding $F_{spr} - x$ curves were obtained. As soon as the concrete starts cracking, the relation between F_{spr} and x ceases to be linear and the slab dissipates energy in the form of plastic strain. The cumulative energy dissipated by the test model through plastic deformations from the beginning of a given i -th seismic simulation up to a given instant t , $(W_p)_i$ can be estimated by integrating the $F_{spr} - x$ loops. The total plastic strain energy dissipated by the concrete at the end of a given i -th seismic simulation will be denoted by $(W_p)_{i,end}$ hereafter.

Superimposed, Fig. 7 shows with solid lines the cumulative plastic strain energy, $(W_p)_i$ of each seismic simulation normalized by its respective value at the end of the simulation $(W_p)_{i,end}$. It can be seen that, in general, there is a reasonably good correlation between the AE energy and the damage on the concrete expressed in terms of cumulative plastic strain energy. Further, for each simulation the ratio K_i between $(E^{AE})_{i,end}$ and $(W_p)_{i,end}$, i.e., $K_i = (W_p)_{i,end} / (E^{AE})_{i,end}$, was calculated. Fig. 8 shows K_i versus the peak acceleration applied to the shake table PA for each seismic simulation and for both types of sensors (VS30 and VS75). An approximate relationship is observed between K_i and PA , which is linear for the VS30 sensors and exponential for type VS75. These relationships can be expressed with the following equations obtained from regression analysis

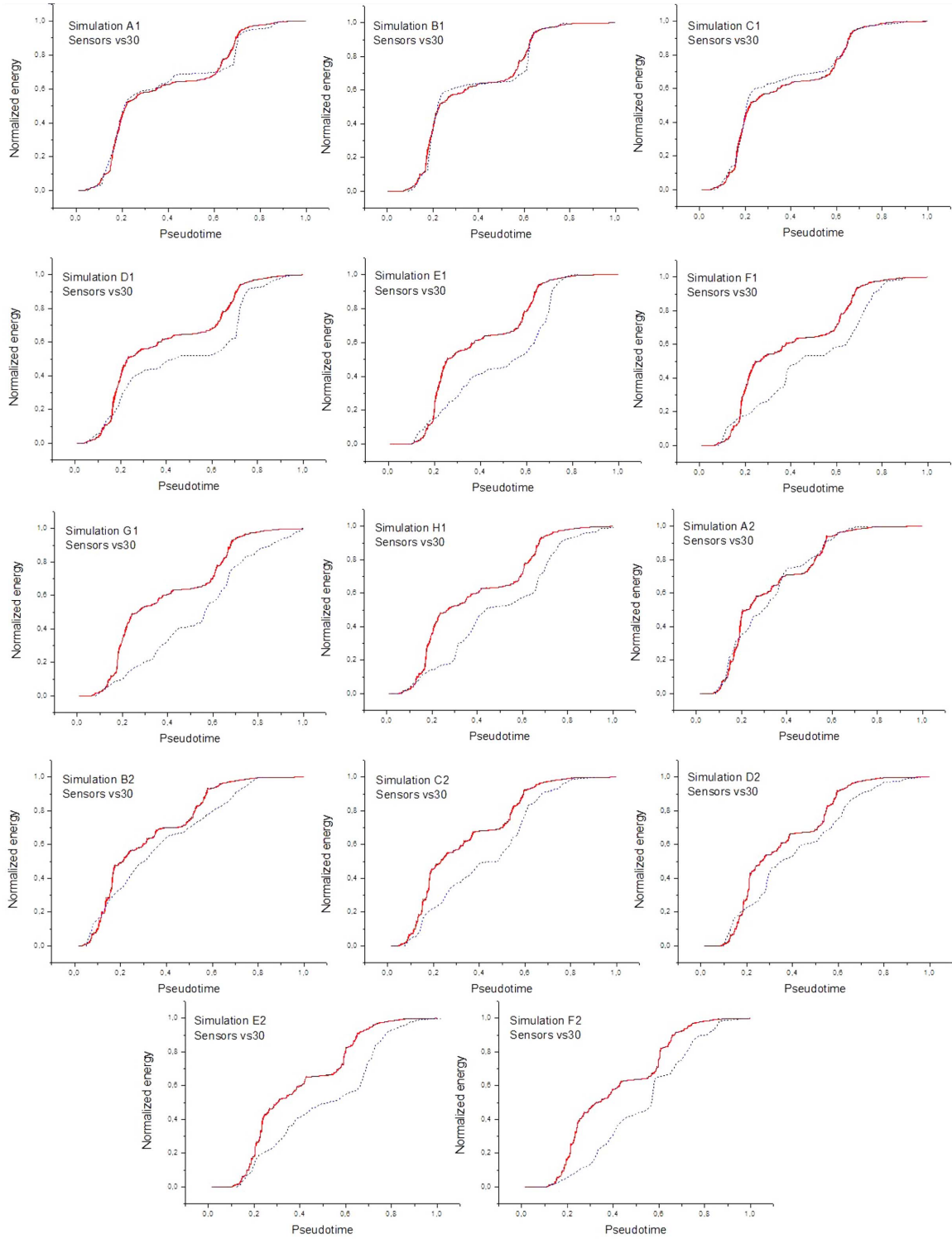


Fig. 7 Normalized $(E^{AE})_i$ (dotted line) and $(W_p)_i$ (solid line) for each seismic simulation (VS30 sensors)

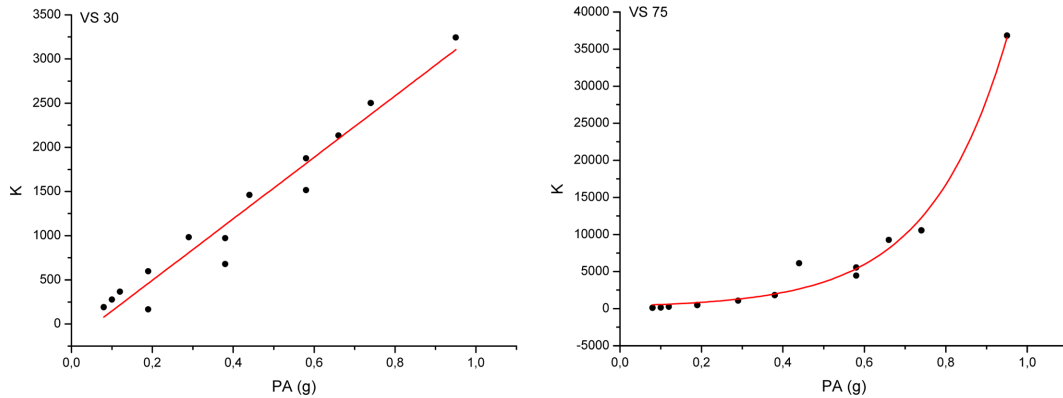


Fig. 8 K versus the PA of each seismic simulation, and its linear regression line. Left: VS30 sensors; Right: VS75 sensors

$$\text{Sensors VS30: } K = 3480.02 \text{ PA} - 200.77 \text{ Nmm/ue; } r = 0.949 \tag{5}$$

$$\text{Sensors VS75: } K = 252.49 \exp(5.23 \text{ PA}) \text{ Nmm/ue; } r = 0.991 \tag{6}$$

where r is the regression coefficient.

The plastic strain energy $(W_p)_i$, is commonly accepted as an appropriate parameter for characterizing low-cycle fatigue damage in RC components, and it is used in well-established RC damage indexes (McCabe and Hall 1989, Park and Ang 1985). The finding that there is a good correlation between $(W_p)_i$, and the AE energy $(E^{AE})_i$, calculated with the AE signals filtered with the procedure proposed in Section 3 would suggest that AE energy can be used as a parameter to quantitatively assess the level of damage in an RC structure subjected to seismic loading. In ongoing research, new damage indexes for RC structures subjected to seismic loadings expressed merely in terms of $(E^{AE})_i$ are intended to be developed on the basis of the findings presented in this paper.

5. Conclusions

The applicability of Acoustic Emission (AE) to assess the damage in reinforced concrete (RC) structures subjected to earthquake loading is investigated. One of the main challenges in applying the AE technique to measurements obtained from such complex dynamic loading is to remove the spurious signals not related to concrete damage. To this end, a procedure is proposed for filtering the raw AE signal. The procedure is applied to the AE measurements obtained from dynamic shake table tests conducted on an RC slab supported on four steel columns. The proposed procedure consists of the application of two filters: **Filter 1** is a polygonal filter over the diagram Amplitude-Duration of the signals; **Filter 2** is based on the calculation of the RMS of the AE signal in different temporal windows. By using these two filters the short-duration signals (associated with concrete fracture and, thus, with cumulative damage to the structure) and the long-duration signals (corresponding to other noisy mechanisms) can be separated. It is found that there is a good correlation between the AE energy calculated with the AE measurements filtered by means of the proposed procedure and the cumulative damage on the concrete measured in terms of cumulative plastic strain energy. Such correlation suggests that the proposed procedure for filtering the AE

signals can be used to develop damage indexes based on AE energy capable of assessing the damage in RC structures subjected to earthquake loads.

Acknowledgements

This research received the financial support of the local government of Spain, *Consejería de Innovación, Ciencia y Tecnología*, Project P07-TEP-02610. The work also received support from the European Union (*Fonds Européen de Développement Régional*).

References

- Benavent-Climent, A., Castro, E. and Gallego, A. (2009), "AE monitoring for damage assessment of RC exterior beam-column subassemblages subjected to cyclic loading", *Struct. Health Monit.*, **8**(2), 175-189.
- Carpinteri, A., Lacidogna, G. and Niccolini, G. (2007), "Acoustic emission monitoring of medieval towers considered as sensitive earthquake receptors", *Nat. Hazard. Earth Sys.*, **7**(2), 251-261.
- Carpinteri, A., Lacidogna, G. and Pugno, N. (2007), "Structural damage diagnosis and life-time assessment by acoustic emission monitoring", *Eng. Fract. Mech.*, **74**(1-2), 273-289.
- Grosse, C. and Ohtsu, M. (2008), *Acoustic emission testing*, Ed., Springer.
- McCabe, S.L. and Hall, W.J. (1989), "Assessment of seismic structural damage", *J. Struct. Eng-ASCE*, **115**(9), 2166-2183.
- McLaskey, G., Glaser, S.D. and Grosse, C.U. (2010), "Beamforming array techniques for microseismic monitoring of large structures", *J. Sound. Vib.*, **329**(12), 2384-2394.
- Miller, R.K. and Hill Eric, V.K. (2005), *Nondestructive Testing Handbook*, 3rd Ed., **6**, Acoustic Emission Testing, Editor: Moore PO ASNT.
- Ministry of Construction of Spain (2002), Spanish Seismic Code NCSE-02. Madrid.
- Ministry of Construction of Spain (2008), Spanish Concrete Code EHE-08. Madrid.
- Ohtsu, M., Okamoto, T. and Yuyama, S. (1998), "Moment tensor analysis of acoustic emission for cracking mechanisms in concrete", *ACI Struct. J.*, **95**(2), 87-95.
- Ohtsu, M. and Watanabe, H. (2001), "Quantitative damage estimation of concrete by acoustic emission", *Constr. Build. Mater.*, **15**(5-6), 217-224.
- Ohtsu, M., Shigeishi, M., Iwase, H. and Koyanagi, W. (1991), "Determination of crack location, type and orientation in concrete structures by acoustic emission", *Mag. Concrete Res.*, **43**(155), 127-134.
- Park, Y.J. and Ang, A.H.S. (1985), "Mechanistic seismic damage model for reinforced concrete", *J. Struct. Eng-ASCE.*, **111**(4), 722-739.
- Yuyama, S., Li, Z.W., Ito, Y. and Arazoe, M. (1999), "Quantitative analysis of fracture process in RC column foundation by moment tensor analysis of acoustic emission", *Constr. Build. Mater.*, **13**(1-2), 87-97.
- Yuyama, S., Li, Z.W., Yoshizawa, M., Tomokiyo, T. and Uomoto, T. (2001), "Evaluation of fatigue damage in reinforced concrete slab by acoustic emission", *NDT&E Int.*, **34**(6), 381-387.
- Zhiwei, L. and Paul, H. (2009), "Evaluation of reinforced concrete beam specimens with acoustic emission and cyclic load test methods", *ACI Struct. J.*, **106**(3), 288-299.